LA-UR -85-2954

LA-UR--85-2954

DE85 017545

Los Alamos National Laboratory is operated by the University of California for the United States Department of Energy under contract W-7405-ENG-36

CONF-860616--1

TITLE HIGH EXPLOSIVE MODELING IN 2D EULER CODE FOR SHAPED CHARGE PROBLEMS

AUTHOR(S) Wen Ho Lee

SUBMITTED TO International Symposium on Intense Dynamic Loading and Its Effects. Beijing, China, June 3-7, 1986

Los Alamos

Los Alamos National Laboratory
Los Alamos, New Mexico 87545

High-Explosive Modeling in 2D Euler Code for Shaped Charge Problems

by

Wen Ho Lee
Computational Physics Group
Applied Theoretical Physics Division
Los Alamos National Laboratory
Los Alamos, New Mexico

Abstract

The object of this study is to incorporate a programmed burn model of high explosive into a two-dimensional, smeared shock Eulerian hydrodynamic code. Huygen's principle and Chapman-Jouguet theory are used in defining the detonation velocity and the location where the high-explosive energy is released. Precalculated burn information such as burn times, burn distances, burn intervals, and burn fractions are implemented into the code before the hydrodynamic actions take place. Two shaped charge problems are tested using the present code and the results are compared with the experimental data, as well as those from other codes.

I. Introduction

Computer simulations for the detonation of high explosive have drawn more attention recently both in industrial applications and laboratory analysis. There are two approaches, namely programmed burn and reactive burn, used in modeling the high-explosive energy release. Programmed burn is easy and stable when it is incorporated with hydrodynamic calculations while the reactive burn model may be more accurate, but more expensive and unstable.

Most of the 2D codes for general engineering design purpose are still using the programmed burn. For example, the 2D Lagrangian codes, HEMP[1], DYNA2D[2], EPIC2[3], MAGEE[4], and the 2D Eulerian codes, HELP[5], HULL[6], and SOIL[7]. Those codes produce good computed results compared with the experimental data although the programmed burn is the only tool for adding the high explosive released energy to the systems.

The present work uses the improved particle-in-cell (PIC) numerical scheme which is second-order accurate in time and space. The PIC method can be interpreted as a Lagrangian calculation (Phase I) followed by an Eulerian remapping (Phase II) back to the original cell locations. The high explosive deposits its energy to the system in Phase I only. Finally, two examples of high-explosive driven metal formation (shaped charge) are shown to demonstrate accuracy of the model.

II. The Operator Splitting and PIC Method

The present work uses operator splitting and particle-in-cell methods to solve the dependant variables such as density, velocity, and internal energy. For a cylindrical coordinate, the governing equations are split into two parts and solved in radial (r) and axial (z) directions separately. In order to maintain a better accuracy, the calculations are alternated in directions for each computational cycle, e.g., r-z-z-r or z-r-r-z. The computational procedures can be briefly described in two phases: In phase 1, known as the

Lagrangian phase, the Lagrangian quantities at the (n+1)th time step are computed based on previous known quantities, i.e., the (n)th time step. In phase 2, known as remap or particle transport phase, the particles are transported according to a "tilde" velocity. The new cell mass (at n+1 time step) is the sum of the masses of the particles in that cell after transport. The new velocity is the final momentum in the cell divided by the new cell mass. The new cell specific internal energy is the final total internal energy divided by the new cell mass.

The partial differential equations for the compressible flow are given below for r and z directions separately.

For the r direction, we have

$$\rho_t = -\bar{u}\,\rho_r - \frac{\rho}{r}(ru)_r \qquad \text{(mass)} \qquad (1)$$

$$u_t = -\bar{u}\,u_r - \frac{1}{\rho}P_r \qquad \text{(r momentum)}, \qquad (2)$$

$$v_t = -\bar{u}\,v_r \qquad \text{(z momentum)}, \qquad (3)$$

and

$$e_t = -\bar{u}\,e_r - \frac{P}{\rho r}(ru)_r + S \qquad \text{(energy)}. \qquad (4)$$

For the z dirction, we have

$$\rho_t = -\bar{v}\,\rho_z - \rho v_z \qquad \text{(mass)}, \qquad (5)$$

$$u_t = -\bar{v}\,u_z \qquad \text{(r momentum)}, \qquad (6)$$

$$v_t = -\bar{v}\,v_z - \frac{1}{\rho}P_z \qquad \text{(z momentum)}, \qquad (7)$$

and

$$e_t = -\bar{v}\,e_z - \frac{P}{\rho}v_z + S \qquad \text{(energy)}. \qquad (8)$$

In Eqs. (1) through (8), ρ is the density, t the time, $\bar{u}$ and $\bar{v}$ the cell edge time average velocities in r and z directions, P the pressure, u and v the velocities in r and z directions, S the energy source due to high explosive, and the subscripts t, r, and z represent the first derivative, i.e., $\frac{\partial}{\partial t}$, $\frac{\partial}{\partial r}$, and $\frac{\partial}{\partial z}$.

In high-explosive programmed burn, the basic assumption is that the detonation wave front travels in all directions at the Chapman-Jouguet detonation velocity. Information concerning the energy released from high explosive such as burn time (BT) and burn interval (BI), are precalculated and stored in the code at time t = 0. During the run, when the problem time T^n, at cycle n, becomes greater than the BT value of a high-explosive cell, but less than (BT + BI), a fraction of the specific energy for the particular HE is deposited in the cell. This fraction is given by $(T^n - BT)/BI$. On the next cycle, at T^{n+1}, if T^{n+1} is still less than (BT + BI), another fraction

$(T^{n+1} - T^{n})/BI$ of specific energy is deposited in the cell. This continues until the cell is completely burned.

The burn calculations depend on the Huygen's construction for the burn distance. In Fig. 1, if A is the detonation point, then the burn distances to points 1 and 2 are the line-of-sight distances from the detonation point, i.e., lines $\overline{A1}$ and $\overline{A2}$. However, the calculation of the burn distance to point 3 is more complex because point 3 is located in the shadow region from point A. In this case, the burn distance is obtained from the shortest distance of the high-explosive wave paths including a new spherical wave centered at point B. One possible solution of the burn distance for point 3 is the total distances of line $\overline{AB}$, chord $\overline{BC}$, and line $\overline{C3}$.

III. Test Problems and the Results

In modeling the test problems, a 2D Lagrangian code was used to initialize the setup and do short time calculation so that the liner will become thicker, which will allow the Eulerian code to have more zones in the liner.

The first test problem is a confined, hemispherical, copper-lined, shaped charge with PBX-W-113 as high explosive. The computational simulation of the charge and the initial conditions are shown in Fig. 2, with the thickness of the aluminum case 0.635 cm and the copper liner 0.47498 cm. The explosive charge was simultaneously initiated at all points along the $\overline{AB}$ plane which is a circular disc. The surfaces along $\overline{HE}$, $\overline{EF}$ and $\overline{GF}$ are treated as continuous flow boundary conditions, while the z-axis as a nonflow, reflective boundary.

The equation of state for the high explosive is the Jones-Wilkins-Lee (JWL) set, which can describe the pressure-volume-energy relation of the detonation products very accurately in involving metal acceleration. The JWL-EOS for the pressure is:

$$P = A\left(1 - \frac{\omega}{R_1 V}\right) e^{-R_1 V} + B\left(1 - \frac{\omega}{R_2 V}\right) e^{-R_2 V} + (\varepsilon - \varepsilon_1)\,\frac{\omega}{V} \qquad (9)$$

where A = 9.50448 MBar, B = 0.10915 MBar, R_1 = 5.0, R_2 = 1.4, ω = 0.40 ε_1 = undetonated HE and ε the detonation energy. In computing the detonation energy released, we also need the following C-J parameters: ρ_o = 1.672 g/cm^3, D = 0.8311 cm/μsec, ε_o = 0.087 MBar - cm^3/cm^3 and $\varepsilon_{chemical} = \varepsilon_o + \varepsilon_1$ = 0.742686 MBar - cm^3/cm^3. The geometry of the collapsing copper liner and the jet formations is given in Figs. 3 through 5. The jet starts to collapse at about 40 μsec after the charge initiation as shown in Fig. 3. At time = 70 μsec, the wings of the jet were bent toward the jet tip direction as a result of the aluminum case. Fig. 5 shows a jet of 34-cm long and with the maximum width of 4-cm near the slug region. The cumulative mass versus velocity plot at time = 100 μsec is shown in Fig. 6 with the tip velocity of 0.50 cm/μsec. The experimental data shows that the tip velocity at time = 100 μsec, is 0.496 cm/μsec. This suggests that the numerical simulation is off by 0.8%.

The second charge studied had a conical, 42° copper liner, 2-mm thick and was loaded with Comp. B. Both experimental and computational charges were confined with aluminum bodies and had cone diameters of 81.3 mm as shown in Fig. 7. The explosive region was detonated by single point initiated at point A for the modeling calculations. Again, we use the JWL EOS. i.e., Eq. (8), with the constants, A = 5.242 MBar, B = 0.07678 MBar, R_1 = 4.2, R_2 = 1.1, ω = 0.34, and ε_1 = 0.2644163 MBar - cm^3/cm^3. The C-J parameters are ρ_o = 1.717

g/cm^3, D = 0.798 cm/μsec, ε_o = 0.085 MBar - cm^3/cm^3, and $\varepsilon_{chemical}$ = 0.3494163 MBar - cm^3/cm^3. The experimental measurements recorded were the collapse angles along the inside and outside surfaces of the liner wall, β^{in} and β^{out} respectively, and the distance, L, from the stagnation point to the rear of the slug. The radiographs of the collalpse process were taken at delay time of 25, 31, and 37 μsec after the initiation of the charge. Due to the detonator/booster assembly in the experiment, there is a difference of 9.5 μsec between the data and calculations. Table I shows the comparisons among the data, HEMP and present codes calculations. The HEMP code calculations and the detail geometry of the shaped charge are reported in Reference 9. The cumulative mass versus jet velocity is plotted in Fig. 8 with tip velocity of 0.73 cm/μsec (experimental data is 0.77 cm/μsec). The present code simulation shows that the jet starts to break at 106 μsec (Fig. 9) as compared to the data of 106.4 μsec [9].

References

1. Wilkins, M. L., "Calculation of Elastic-Plastic Flow," in Alder, B. et. al. (eds.) Method in Computational Physics, (Academic Press, New York) pp 211-264 (1964).

2. Hallquist, J. O., "DYNA2D - An Explicit Finite Element and Finite Difference Code for Axisymmetric and Plane Strain Calculations (Users Guide)," University of California, Lawrence Livermore National Laboratory, Report UCRL-52429 (1978).

3. Johnson, G., "Recent Developments and Analyses Associated with the EPIC-2 and EPIC-3 Codes," in Advances in Aerospace Structures and Materials, S. S. Wang and W. J. Renton. eds., ASME Publ. No. Ad-01, 1981.

4. Kolsky, H. G. "A Method for the Numerical Solution of Transient Hydrodynamic Shock Problems in Two Space Dimensions," Los Alamos Scientific Laboratory Report LA-1867 (1955).

5. Hageman, L. J. et. al., "HELP, A Multi-material Eulerian Program for Compressible Fluid and Elastic-Plastic Flows in Two-Dimensions and Time," Systems, Science and Software Report SSS-R-75-2654, July 1975.

6. Durrett, R. E. and D. A. Matuska, et. al., "The HULL Hydrodynamics Computer Code," Air Force Weapons Laboratory, AFWL-TR-76-183, September 1976.

7. Johnson, Wallace E., "Modifications of OIL-Type Computer Programs," BRL Contract Report ARBRL-CR-0476, Ballistic Research Laboratory (January 198[illegible]).

8. Simmons, B. M. "A Study of Shaped-Charge Collapse and Jet Formation using the HEMP Code and A Comparison with Experimental Observations," BRL-MR-3417, Ballistic Research Laboratory (December 1984).

9. Simon, J. "The Effect of Explosive Detonation Characteristics on Shaped Charge Performance," BRL-MR-2414, Ballistic Research Laboratory (September 1974).

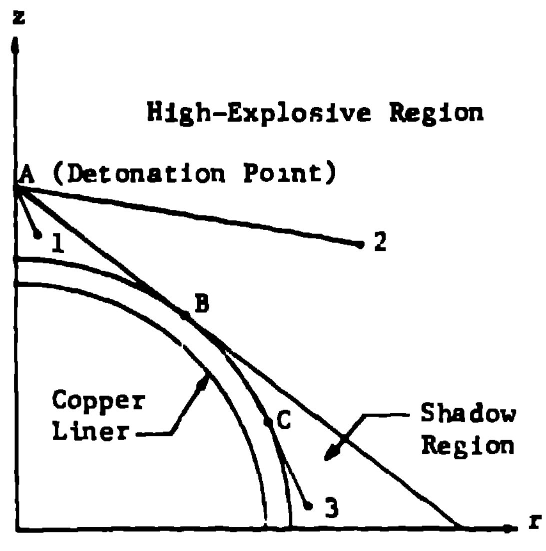

Fig. 1. Huygen's Construction for Burn Distances

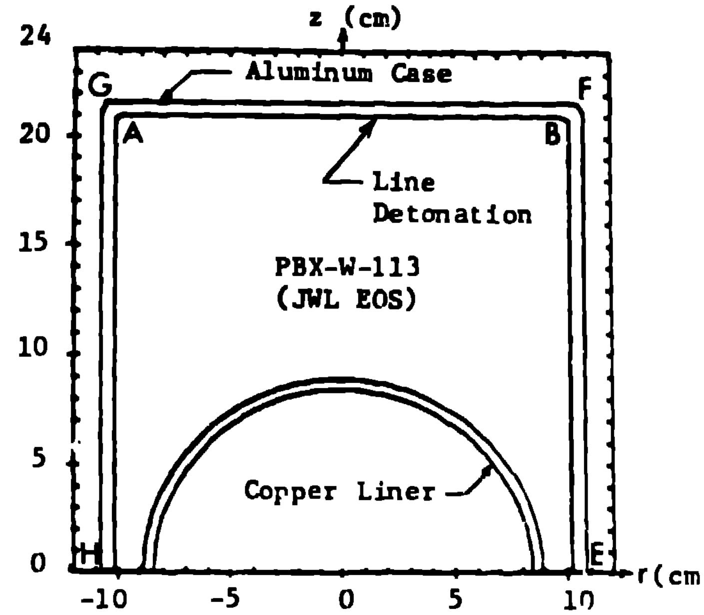

Fig. 2. Initial Geometry of First Test Problem

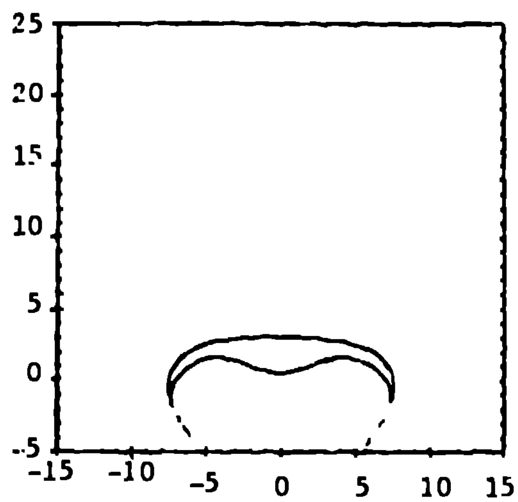

Fig. 3. Jet Shape at time = 40 µsec

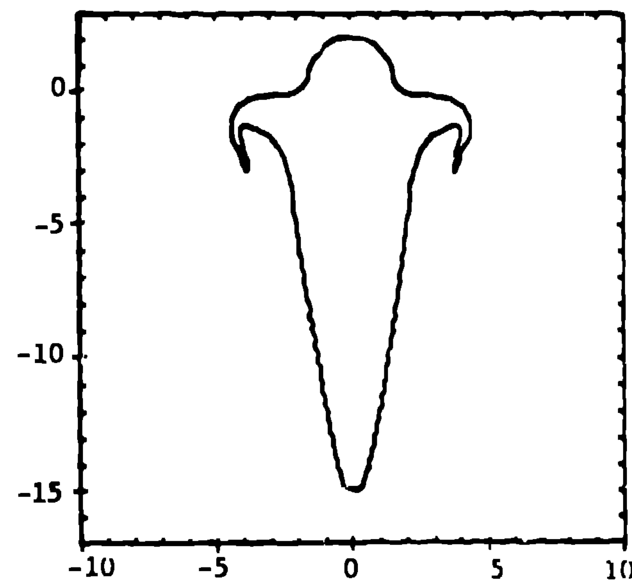

Fig. 4. Jet Shape at time = 70 µsec

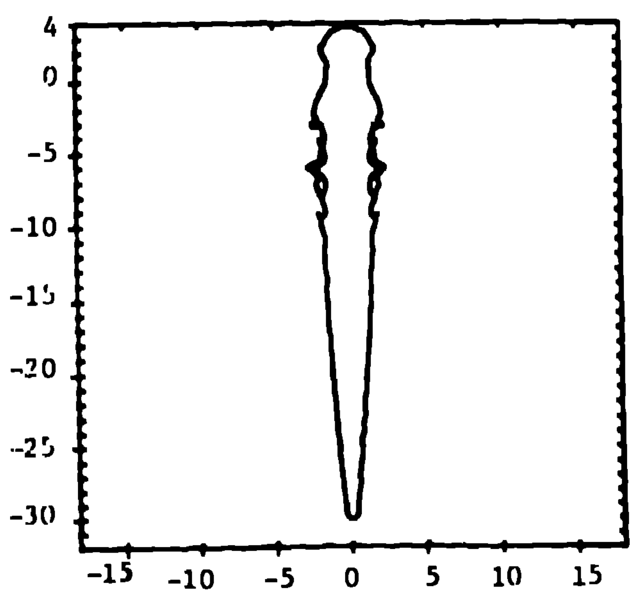

Fig. 5. Jet Shape at time = 100 µsec

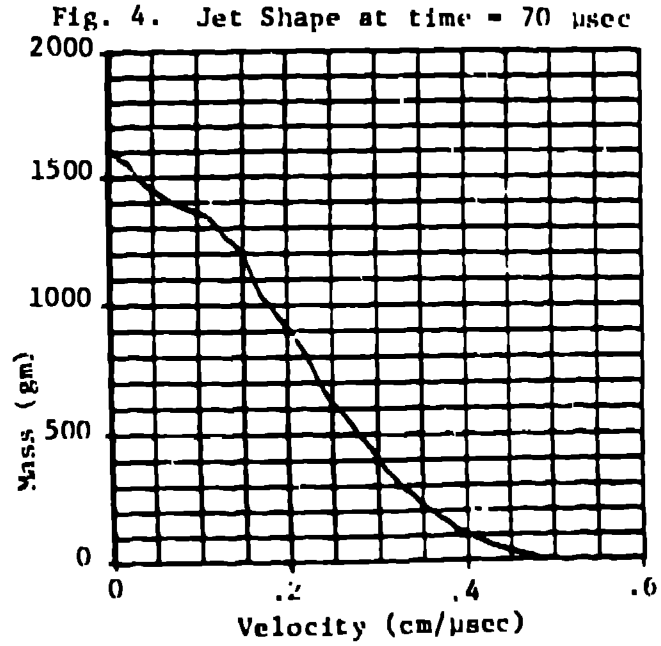

Fig. 6. Cumulative Mass versus Velocity at time = 100 sec

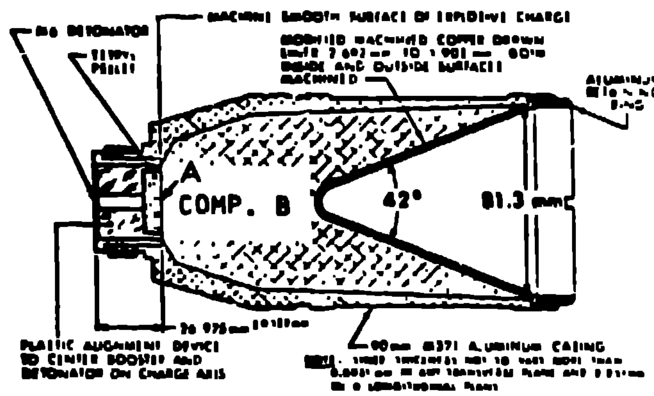

Fig. 7. Sketch of 81.3 mm BRL Precision Charge

TABLE 1.

COLLAPSE SEQUENCE FOR A 42° COMP. B CHARGE -
X-RAY OBSERVATIONS VS. CODE CALCULATIONS

	Elapsed Time	Collapse Angle		L *
1) X-Rays	25.0μs	$\beta^{in} = 35°$,	$\beta^{out} = 32°$	20mm
HEMP	15.5μs	$\beta^{in} = 35°$,	$\beta^{out} = 32°$	26mm
PRESENT STUDY	15.5μs	$\beta^{in} = 35°$	$\beta^{out} = 32°$	21mm
2) X-Rays	31.0μs	$\beta^{in} = 42°$,	$\beta^{out} = 39°$	44mm
HEMP	21.5μs	$\beta^{in} = 42°$,	$\beta^{out} = 36°$	50mm
PRESENT STUDY	21.5μs	$\beta^{in} = 42°$	$\beta^{out} = 39°$	45mm
3) X-Rays	37.0μs	$\beta^{in} = 53°$,	$\beta^{out} = 49°$	58mm
HEMP	27.5μs	$\beta^{in} = 54°$,	$\beta^{out} = 47°$	76mm
PRESENT STUDY	27.5μs	$\beta^{in} = 53°$	$\beta^{out} = 49°$	68mm

$\Delta t = 9.5 \mu s$

* L is the distance from the stagnation point to the rear of the slug.

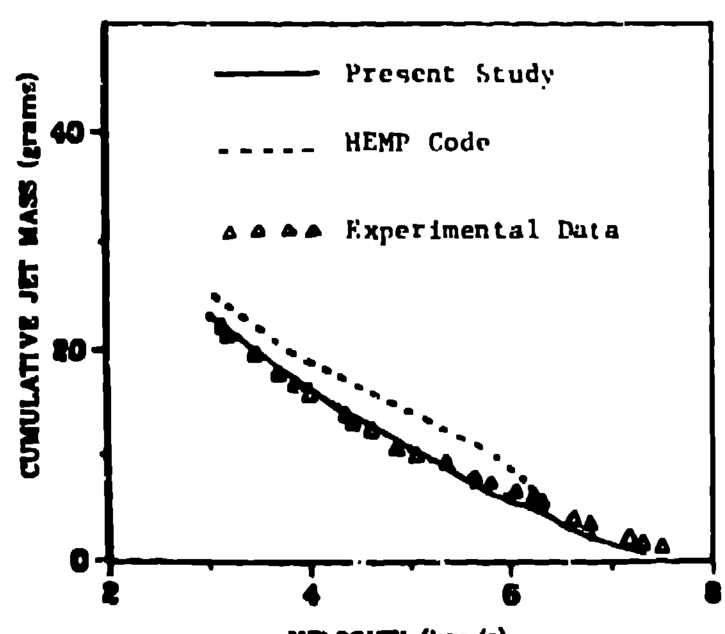

Fig. 8. Mass vs. Velocity Plot for Present Study, HEMP and Data

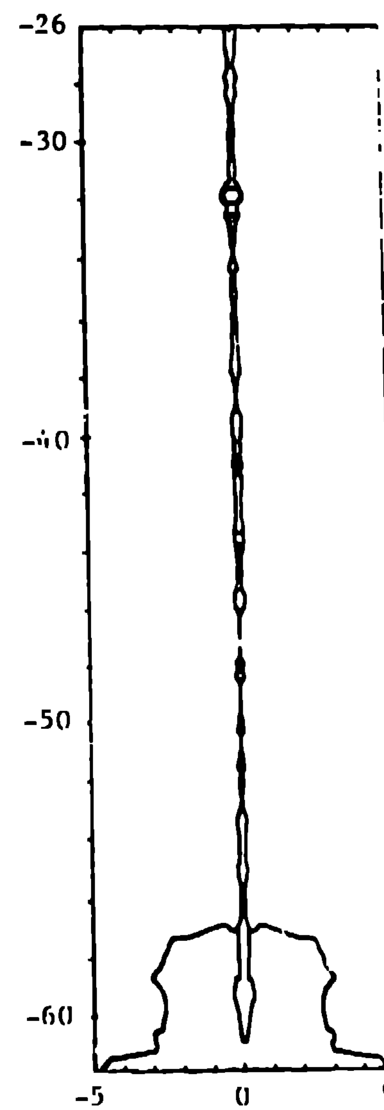

Fig. 9. The Jet Starts to Break at time = 106 μsec (only 24.2 gm of Jet are shown).